JOURNAL OF SOLID STATE CHEMISTRY 45, 14–39 (1982)

Study of Electron States of Solids by Techniques of Electron Spectroscopy*,†

C. N. R. RAO‡ AND D. D. SARMA

Solid State and Structural Chemistry Unit, Indian Institute of Science, Bangalore-560012, India

Received March 31, 1982

Studies of valence bands and core levels of solids by photoelectron spectroscopy are described at length. Satellite phenomena in the core level spectra have been discussed in some detail and it has been pointed out that the intensity of satellites appearing next to metal and ligand core levels critically depends on the metal–ligand overlap. Use of photoelectron spectroscopy in investigating metal–insulator transitions and spin-state transitions in solids is examined. It is shown that relative intensities of metal Auger lines in transition metal oxides and other systems provide valuable information on the valence bands. Occurrence of interatomic Auger transitions in competition with intraatomic transitions is discussed. Applications of electron energy loss spectroscopy and other techniques of electron spectroscopy in the study of gas–solid interactions are briefly presented.

Introduction

Techniques of electron spectroscopy have become the principal means for investigating electron states in atoms, molecules, solids, and surfaces (*1*, *2*). Basically, all these techniques involve analysis of the kinetic energy of the ejected or scattered electrons. Some of the important techniques of electron spectroscopy employed to study solids are photoelectron spectroscopy using X-ray or uv radiation, Auger electron spectroscopy, and electron energy loss spectroscopy (*1*–*5*). While uv photoelectron spectroscopy (uvPS) provides valuable information about the valence bands of solids, X-ray photoelectron spectroscopy (XPS) is a probe for both valence bands and core levels. Auger electron spectroscopy (AES) can also be fruitfully employed for probing valence bands as well as core levels. Electron energy loss spectroscopy (EELS) has become extremely popular in recent times in the study of surfaces. Applications of EELS to surfaces have been recently reviewed by Rao *et al.* (*6*). In this article, we shall briefly discuss the applications of some of the techniques of electron spectroscopy for investigating electron states of solids, taking most of the examples from our investigations.

* Presented at the Symposium on the Electronic Structure and Bonding in Solids, 183rd National Meeting, American Chemical Society, held in Las Vegas, Nevada, March 30–31, 1982.

† Communication No. 181 from the Solid State and Structural Chemistry Unit.

‡ To whom all correspondence should be addressed.

Valence Bands

Photoelectron spectroscopy has been extensively used in the study of valence bands of solids. Photoemission of an electron from a solid can be described in terms of a three-

0022-4596/82/130014-26$02.00/0

step process (*7*): excitation of the electron from an initial state to a final state, transport of the electron to the surface of the solid, and ejection from the surface. The final state is a vacant band whose shape is determined by the crystal potential. If the energy of the electron is fairly high, so that the final state of the electron corresponds to a state far above the Fermi level, the final state can be approximated by an unstructured continuum and the photoelectron spectrum will correspond to the density of states of the initial state. Radiation of energy greater than 30 eV is generally sufficient to promote the electron to an unstructured final state (*8*) and the experimental photoelectron spectrum then corresponds to the calculated density of states. For this reason, X-ray as well as He II ($h\nu$ = 40.8 eV) photoelectron spectra of solids can be directly related to the density of states. Such comparisons have been made for a number of metals. Of the alkali metals, Na is considered to have the freest electrons and XPS of Na valence band shows the expected $E^{1/2}$ dependence of intensity (*9*). XPS of the $4d$ metals show excellent agreement with the theoretically calculated densities of states (*10*). The agreement between the observed and calculated densities of states is reasonable for the $5d$ metals (Ir, Pt, and Au), although there is some evidence of modulation of spectral intensities in the low-energy region by transition matrix elements (*10*).

At lower excitation energies ($h\nu < 30$ eV), the final state is likely to be heavily structured and photoelectron spectra will correspond to the joint density of states of the initial and the final states. In this energy range of excitation, spectral features vary with the excitation energy (*7, 8*). Theoretically evaluated joint densities of states have been compared with photoelectron spectra at low excitation energies for transition metals like Rh, Pd, Ag, Ir, and Pt and the agreement is reasonable (*11*).

Study of valence bands in alloys using electron spectroscopic techniques has given information concerning the nature of bonding in alloys (*12*). Using these techniques it has been possible to obtain answers regarding the applicability of the rigid band model, coherence potential approximation, and so on. In most alloys of transition metals, individual d bands of the component metals retain their characteristic structures; however, evidence of small mutual perturbations has been found. These examples have amply demonstrated the inadequacies of the rigid band model of alloys. Coherent potential approximation provides better agreement with experimental observations.

Valence band spectra of transition and rare earth metals, as well as their compounds, show structures due to final state effect. In the case of transition metal compounds, the d-level occupancy of the metal ion changes from n to $(n-1)$ following the photoionization. Consequently, the final state must correspond to one of the multiplets available to d^{n-1} configuration; the probability of occupying any particular multiplet is given by the fractional parentage coefficients (*13*). Thus the structure seen in the valence band regions of the spectra corresponds to multiplets available to the d^{n-1} configuration, while intensities of these structures are given by fractional parentage coefficients. In Table I, we show final states of a few typical transition metal ions. We illustrate this final state effect in the valence bands of iron oxides in Fig. 1, which exhibit various multiplets. Energies of these multiplets compare well with those calculated by Alvarado *et al.* (*13a*) on the basis of a single ion in a crystal field approximation. Similar structures can be seen in the $4f$-level spectra of rare earth metals and their compounds corresponding to the multiplets of f^{n-1} configurations (Fig. 2).

Using radiations with different energies, it has been possible to separate the d-like

TABLE I

FINAL STATE TERMS AND ENERGIES FOR A FEW TRANSITION METAL IONS

Ion	Final state term	Experimental energy (eV)
Fe^{2+}	$^6A_{1g}$	0.5
	$^4T_{1g}$, $^4T_{2g}$	3.5
	$^4T_{1g}$, $^4T_{2g}$, ^4E_g	5.5
Co^{2+}	$^5T_{2g}$, $^3T_{1g}$, $^3T_{2g}$	1.8
	$^3A_{2g}$, ^3E_g, $^3T_{2g}$, $^3T_{1g}$	3.8
Ni^{2+}	$^4T_{1g}$	1.7
	^2E_g	2.3
	$^2T_{1g}$	3.9

bands and p-like bands in the valence band spectra of Cr_2O_3, MnO, FeO, CoO, and NiO (*14*), as the cross sections of photoionization of d and p levels have different dependence on the excitation energies. In these cases, d-like bands could be analyzed in terms of final state effects. A study of the first-row transition metal monosulfides (*15*) has enabled assignments of metal $3d$ and sulfur $3p$ bands in the valence region spectra (Fig. 3). Electronic properties of these sulfides have been explained on the basis of the location of $E(3d)$ with respect to E_f.

Comparison of band structure calculations and photoelectron spectra in the valence band regions have been carried out for various nonmetallic systems. For example, Shevchick *et al.* (*16*) have compared calculated densities of states with observed valence bands in a host of III–V and II–VI crystalline and amorphous semiconductors. Similar studies on layer compounds (like $SnSe_2$, PbI_2, BiI_3, and GaSe) (*17*) and gallium chalcogenides (*18*) show good agreement between experiment and theory. Studies of valence bands by photoelectron spectroscopy have been reviewed by several authors; in particular, the articles by Green (*19*) and Watson and Perlman (*12*) are instructive.

Core Levels

Binding energies of core levels obtained from photoelectron spectra of metal compounds are characteristic of the extent of

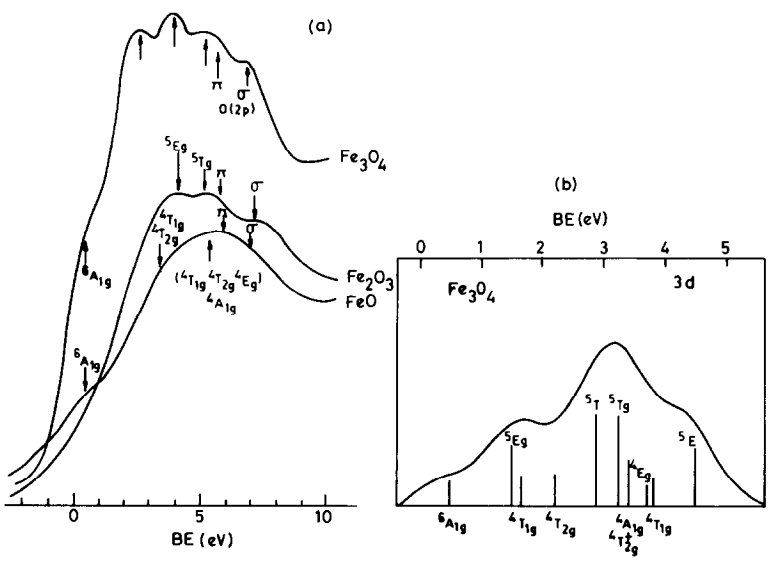

FIG. 1. (a) He II spectra of FeO, α-Fe_2O_3, and Fe_3O_4 showing the final state multiplet structures of $3d$ levels. (b) Theoretical spectrum of Fe_3O_4 calculated in terms of the final states of the component ions, Fe^{2+} and Fe^{3+}, in single-ion-in-crystal-field approximation [after Ref. (13a)].

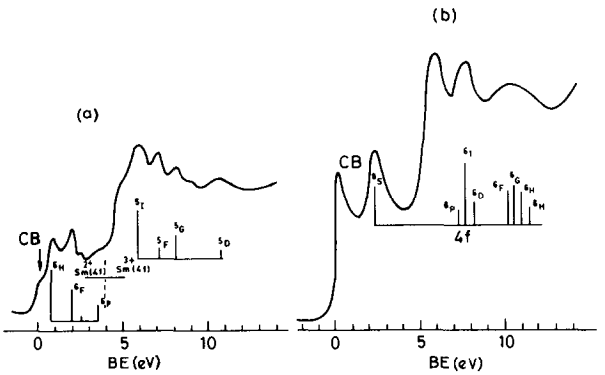

FIG. 2. He II spectra in the valence band regions showing the final state effects in (a) Sm and (b) Tb. The valence band of Sm shows the coexistence of both divalent and trivalent species due to valence instability.

charge transfer from the metal to the ligand. In Fig. 4, we have plotted the binding energies of various metal core levels in related series of oxides of Ti, V, Cr, and Mn against the formal oxidation number of the metal. We see that the binding energies increase with the oxidation state of the metal. This chemical shift can be attributed to a decreased interelectronic repulsion with increasing oxidation state owing to a greater charge transfer from the metal to the ligand. However, the decrease in interelectronic repulsion is partly offset by the Madelung energy term and the observed increase in binding energy is, therefore, not as large. Relaxation energy following photoionization can also modify the observed chemical shift to a considerable extent; however, this term is not likely to vary drastically from one oxidation state to another.

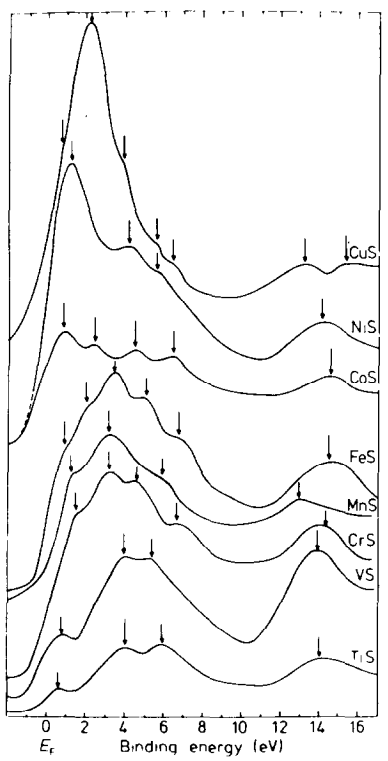

FIG. 3. X-Ray photoelectron spectra of valence bands in first-row transition metal monosulfides. Arrows show various peak positions. Peaks in the 14-eV region are due to sulfur (3*s*).

Chemical shifts (ΔE) of X-ray absorption edges of transition metal compounds have been studied in some detail. The chemical shifts, ΔE, in a series of compounds of a transition metal are related to the effective charge on the metal ion, q, as $\Delta E = aq + bq^2$, where a and b are constants. This relation has been justified on theoretical considerations as well (*20*). Binding energies of core levels of compounds of a given transition metal are linearly related to ΔE from X-ray absorption edge measurements as shown in Fig. 5. This suggests that core level binding energies can themselves be re-

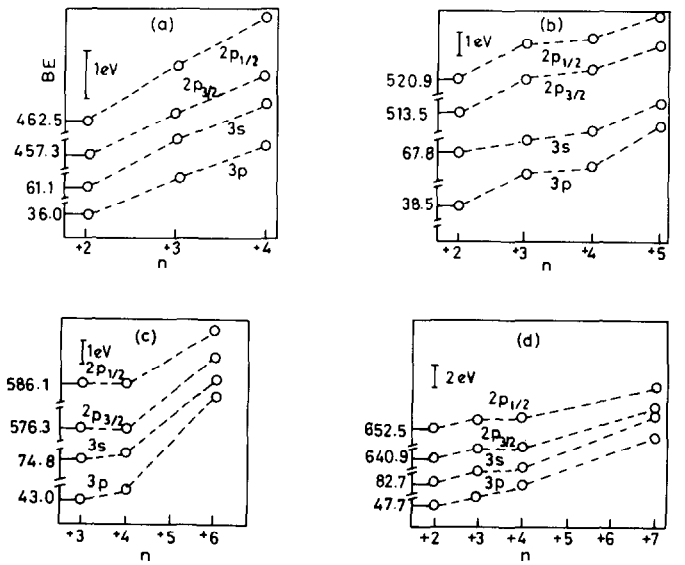

FIG. 4. Variation of $3p$, $3s$, and $2p$ binding energies of first-row transition metal oxides with the oxidation state, n, of the metallic ion: (a) Ti; (b) V; (c) Cr; and (d) Mn.

lated to q by the expression $aq + bq^2$.

The hole spectrum of any core level with finite orbital angular momentum ($1 \neq 0$) shows a doublet structure due to spin–orbit coupling in the absence of any strong interaction of the core-hole with the valence electrons. The magnitude of the spin–orbit splitting, ΔE_{nl}, of the level (nl) can be expressed in terms of the Dirac equation with an effective nuclear charge $(Z - Z_0)$ replacing the nuclear charge, Z. The relationship between ΔE_{nl} with $(Z - Z_0)$ is approximated from the Dirac equation as $\Delta E_{nl} \propto (Z - Z_0)^4$. This relationship seems to be valid for many levels (*21*). However, in oxides and sulfides of first-row transition metals, ΔE_{2p} is found to vary linearly with Z (Fig. 6). Such large deviations from the variation expected from the Dirac equation are found in the data of several levels of transition metal compounds (*22*). These deviations can be explained in terms of the dependence of the screening constant on several types of interaction of the core-hole with other electrons, including the valence electrons. This indicates that any drastic change in valence band due to changes in the bonding will be reflected in the spin–orbit splittings (via Z_0). Thus spin–orbit splitting is found to decrease considerably when a transition metal system undergoes a transition from the high-spin to the low-spin configuration. Similarly, the spin–orbit splitting varies systematically with the oxidation state of transition metal, the d^0 configuration of the metal showing a large decrease.

The s-level spectra of compounds of transition metals (including rare earths) show a doublet structure (Fig. 7), although the orbital angular momentum of the core level is zero. This doublet structure arises primarily from the exchange interaction of the metal electrons in the d (or f level) with the core-hole. This process can be represented by

$$[ns^2(^1S)\ V^m(^{2s+1}L)]-{}^{2s+1}L \xrightarrow{h\nu} [ns^1(^2S)\ V^m(^{2s+1}L)]\left\{{}^{2s}L,\ {}_{2(s+1)}L\right.$$

The strength of this interaction is given by

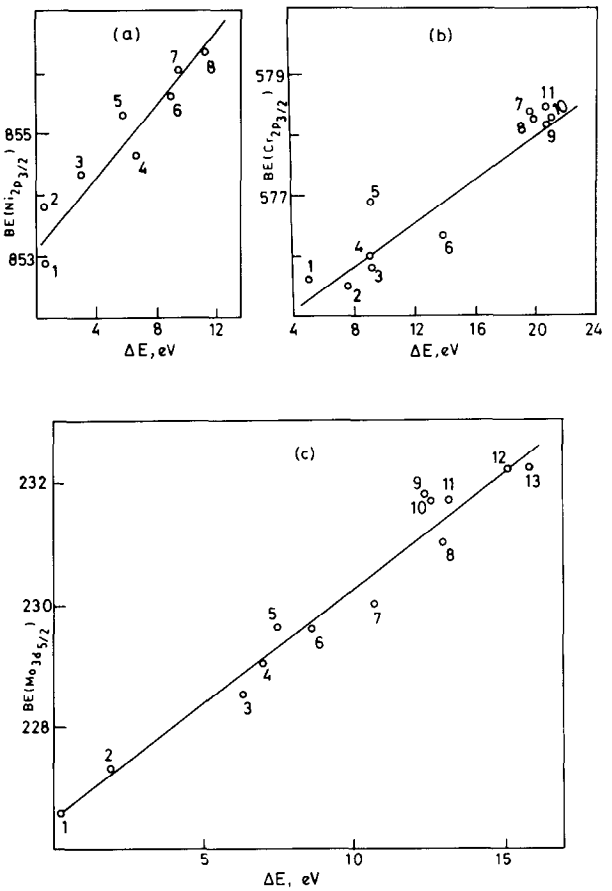

FIG. 5. Plots of metal ($2p_{3/2}/3d_{5/2}$) binding energies from XPS against chemical shifts of the K-absorption edge, ΔE, for (a) nickel compounds: 1. NiI_2; 2. $Ni(PPh_3)_2(CO)_2$; 3. $NiBr_2$; 4. NiO; 5. $NiCl_2 \cdot 6H_2O$; 6. $K_2\,Ni(CN)_4$; 7. $Zn\,Ni(CN)_4$; 8. $NiSO_4$. (b) Chromium compounds: 1. CrS; 2. Cr_2S_3; 3. $NaCrO_2$; 4. $LaCrO_3$; 5. Cr_2O_3; 6. CrO_2; 7. $Cs_2Cr_2O_7$; 8. $Na_2Cr_2O_7$; 9. CrO_3; 10. $K_2Cr_2O_7$; 11. K_2CrO_4. (c) Molybdenum compounds: 1. $Mo(CO)_6$; 2. $MoSe_2$; 3. MoS_2; 4. $MoCl_3$; 5. $(NH_4)_2MoS_4$; 6. $MoCl_4$; 7. $MoCl_5$; 8. $MoO_2(acac)_2$; 9. Ce_2MoO_6; 10. $GdMoO_4$; 11. $H_{0.36}MoO_3$; 12. MoO_3; 13. $SrMoO_4$. Full lines are the least-squares fits of the data.

G^3 (ns, md) or $G^3(ns, mf)$ Slater integrals. This scheme indicates that the intensity ratio of the two peaks in the doublet structure should be proportional to the ratio of the multiplicities of the final states, $(s + 1)/s$, and that the exchange splitting (separation between the doublet structure), ΔE_{ns}, should increase monotonically with the number of unpaired electrons in the d or f shell. Experimentally, one does find the expected variation of ΔE_{ns} with number of unpaired electrons as is illustrated in Fig. 8. From this figure, we see that ΔE_{3s} is maximum for the d^5 configuration of transition metal ions; ΔE_{4s} and ΔE_{5s}, likewise, become maximum for the f^7 configuration of the rare earth ion. This indicates that ΔE_{ns} will be considerably different between various oxidation states of the metal as different oxidation states will have different occupancies of the valence band. Thus, ΔE_{3s} is zero for the d^0 configuration in Cr and Mn compounds and increases with the increase in number of d electrons (Fig. 9). The ex-

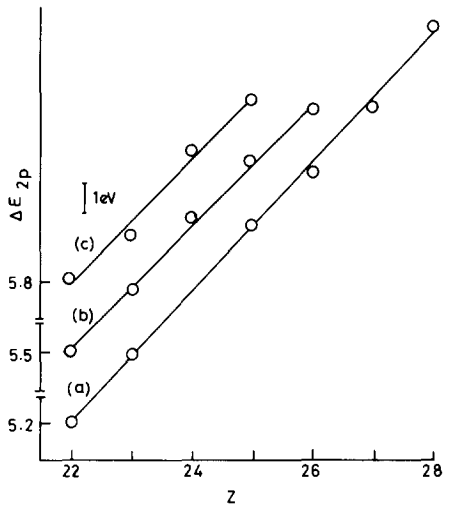

FIG. 6. Variation of the spin–orbit splitting, ΔE_{2p}, of the $2p$ level with the nuclear charge, Z, in (a) monoxides, (b) sesquioxides, and (c) dioxides of first-row transition metals.

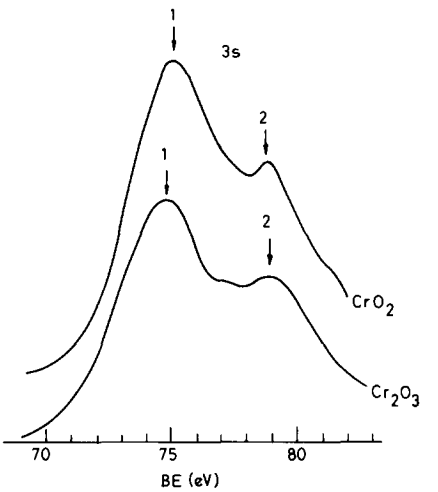

FIG. 7. X-Ray photoelectron spectra of $3s$ regions of Cr_2O_3 and CrO_2 showing the exchange interaction split peak (2) on the higher binding energy side of the main $3s$ peak (1).

change splitting decreases drastically when a transition metal complex undergoes a high-spin to low-spin transition (*23*).

Although variations of ΔE_{ns} mentioned above are observed qualitatively, exact quantitative agreement between the simple

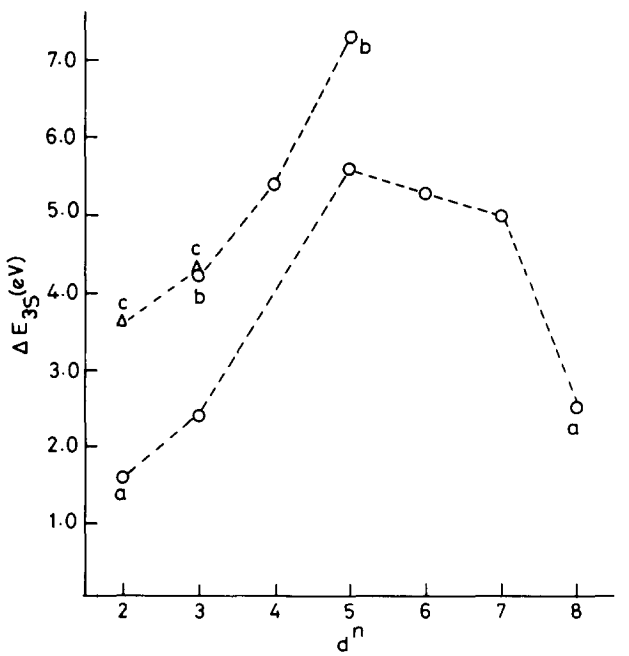

FIG. 8. Variation of the exchange splitting, ΔE_{3s}, of the $3s$ level in first-row transition metal oxides with the number, d^n, of d electrons: (a) monoxides; (b) sesquioxides; and (c) dioxides.

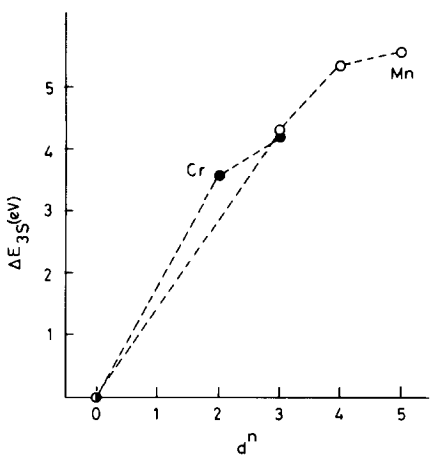

FIG. 9. Variation of the exchange splitting, ΔE_{3s}, in the $3s$ level of Cr and Mn oxides with the number, d^n, of d electrons.

theory and experiment is rather lacking. Thus the ΔE_{ns} evaluated according to $G^3(ns, mf)$ gives quantitative agreement only in the case of the $5s$ level of rare earth ions, while grossly overestimating the exchange splitting in other cases (*24*). Intensities of the two exchange interaction split peaks are in most of the cases different from what should be expected on the basis of multiplicities of the two states alone. These differences are likely to be due to configuration interaction between various other states where the symmetry of the state is the same as that of the exchange split peaks (^{2s}L or $^{2(s+1)}L$). While suppressing the magnitude of the exchange splitting in the $3s$ and $4s$ levels considerably, configuration interaction can lead to an extended multiplet structure (over ~40 eV range) in the s-level spectra instead of a simple exchange split doublet structure (*21, 25*). We have seen such extended multiplet structure in the $3s$ spectra of MnO and CoO (Fig. 10), $4s$ level of RuO_2, and $5s$ levels of HfO_2, Ta_2O_5, and WO_3. Such multiplet structures have also been observed in halides and oxides of other transition metals. We have carried out extensive configuration interaction calculations allowing for $3p^2 \rightarrow 3s3d$ double excitations on various transition metal ions (*25*). These calculations indicate that most of the structure seen in the $3s$-level spectra of the transition metal compounds can be assigned to various configuration interaction states, including those arising from the double excitations $3p^2 \rightarrow 3s3d$. In Table II, we show typical assignments and intensities in the case of Mn^{2+} and Co^{2+}. It is noteworthy that HfO_2, Ta_2O_5, and WO_3 are all d^0 systems and thus cannot lead to any exchange interaction split peak without the inclusion of configuration interaction via the double excitations $5p^2 \rightarrow 5s5d$.

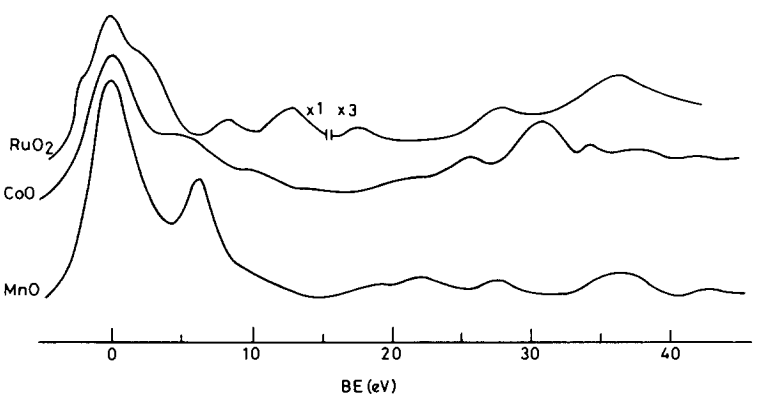

FIG. 10. X-Ray photoelectron spectra of the $3s$ levels of MnO and CoO and $4s$ level of RuO_2 showing the extent of configuration interaction multiplet structures. Binding energy (BE) scale indicates only the relative energy positions of various peaks.

TABLE II

SEPARATION OF MULTIPLET STRUCTURE PEAKS (IN eV) FROM THE MAIN 3s PEAK

	MnO			CoO		
Peak No.	Configuration	Calculated[a]	Observed	Configuration	Calculated[a]	Observed
1.	$^7S(3s^1 3p^6 3d^5)$	0.0 (100)	0.0	$^5F(3s^1 3p^6 3d^7)$	0.0 (100)	0.0
2.	$^5S(3s^1 3p^6 3d^5)$	4.5 (47.5)	6.2	$^3F(3s^1 3p^6 3d^7)$	3.4 (47.3)	4.8
3.	$^5S(3s^1 3p^6 3d^5)$	22.1 (11.2)	22.2	$^3F(3s^2 3p^4 3d^8)$	25.2 (5.2)	25.7
4.	$^5S(3s^2 3p^4 3d^6)$	23.3 (3.0)	27.5	$^3F(3s^2 3p^4 3d^8)$	31.6 (1.2)	34.4
5.	$^5S(3s^2 3p^4 3d^5 4s^1)$	41.2 (1.0)	36.3			

[a] Values in parentheses indicate the calculated relative intensities.

Extended multiplet structures are found in the $4d$ spectra of rare earth metals and their compounds (Fig. 11) (*22*, *26*). The presence of both spin and orbital angular momentum in the core, as well as the valence band, is responsible for these structures. Calculations based on $4d^0 \leftrightarrow 4f^n$ interactions in the intermediate coupling scheme involving sudden approximation (*26*) show fair agreement with experimental spectra (Fig. 11). In the absence of this interaction, $4d$ levels of these compounds would have shown only the spin–orbit split doublet structure. Thus the $4d$ levels of La ($4f^0$) and Lu ($4f^{14}$), both in ^1S state, show only the $4d_{5/2}$, $4d_{3/2}$ doublet structure. However, the $4f^{13}$ configuration (^2F) of Yb_2O_3 gives rise to an extended multiplet structure in the $4d$ level, in contrast with the spectra of $4f^{14}$ configuration (^1S) of Yb which shows the spin–orbit doublet (*27*).

One of the useful applications of the

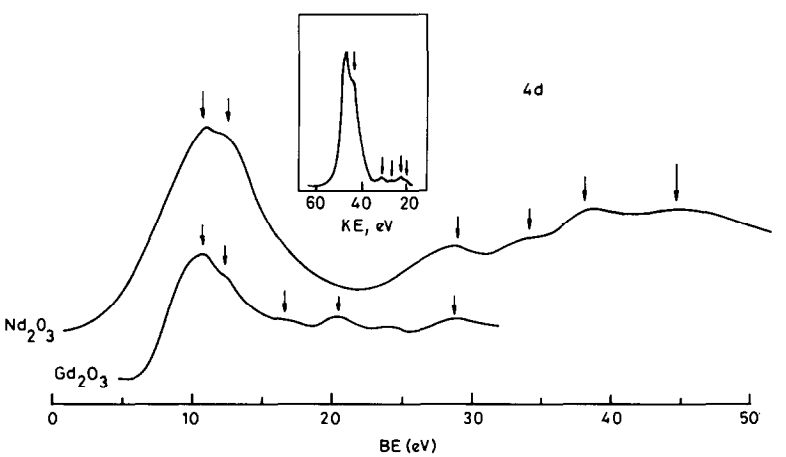

FIG. 11. X-Ray photoelectron spectra of the $4d$ regions of Nd_2O_3 and Gd_2O_3 showing multiplet structures. The $4d$ spectrum of Nd_2O_3, previously calculated [Ref. (*26*)], is shown as an inset. Binding energy (BE) scale indicates only the relative energy positions of various peaks.

chemical shift is in the realm of mixed valence compounds In Fig. 12, we show typical spectra of Magnéli-phase oxides of Ti and V; and in Fig. 13, we show spectra of mixed valence spinel oxides of Mn, Fe, and Co. In Fig. 12, we can clearly see features of both 3+ and 4+ states of Ti and V. It has been possible to assign these peaks to the two oxidation states by comparing the spectra with those of the corresponding sesquioxides and dioxides. Similarly, in the case of the spinel oxides of Mn and Fe, it is possible to assign the features seen in Fig. 13 to 2+ and 3+ oxidation states of the metal by comparing the spectra with those of the mono- and sesquioxides of the metals; Fe^{2+} and Fe^{3+} in Fe_3O_4 cannot be identified by Mössbauer spectroscopy at room temperature due to the time scale of the experiment. The case of Co_3O_4 is somewhat different in that the binding energies observed in this case were lower than those for CoO. This is most probably due to a drastic modification in the relaxation energy in going from CoO to Co_3O_4. However, the features due to 2+ and 3+ species of Co are clearly discernible in the spectra of Co_3O_4. Furthermore, it is noteworthy that the 3*s* spectrum of Co_3O_4 shows only exchange splitting due to the 2+ state of Co, confirming that the 3+ state of Co in Co_3O_4 is in the low-spin configuration.

Satellites in X-Ray Photoelectron Spectra

Satellite phenomena are of common occurrence in X-ray photoelectron spectroscopy and satellites have been reported in the spectra of a variety of compounds. Occurrence of satellites, their intensities, and energy separation from the main core level peak are highly dependent on the nature of bonding of the metal ion to the ligand. Thus oxides, halides, and a few other compounds of first-row transition metals, such as Mn, Fe, Co, Ni, and Cu, show satellites 4–8 eV away from their metal core level spectra (*21*); however, satellites are not seen in the spectra of sulfides (*15*) or low-spin complexes of these metals (*23*). Furthermore, compounds of first-row transition metals preceding Mn show satellites only as very weak features; in TiO_2, for example, a weak satellite can be seen 14 eV away from the main core level peak (*21*). We have found that oxides of some of the second- and third-row transition metals exhibit weak satellites around 14–16 eV from the main metal core level peaks. Oxides and halides of rare earths generally show satellites

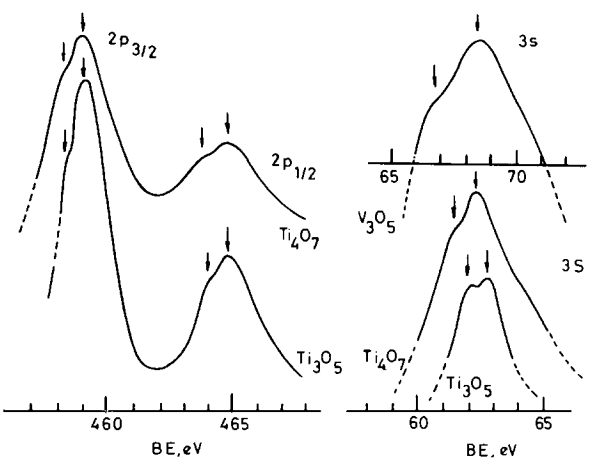

FIG. 12. Typical X-ray photoelectron spectra of a few levels in mixed valence oxides of Ti and V.

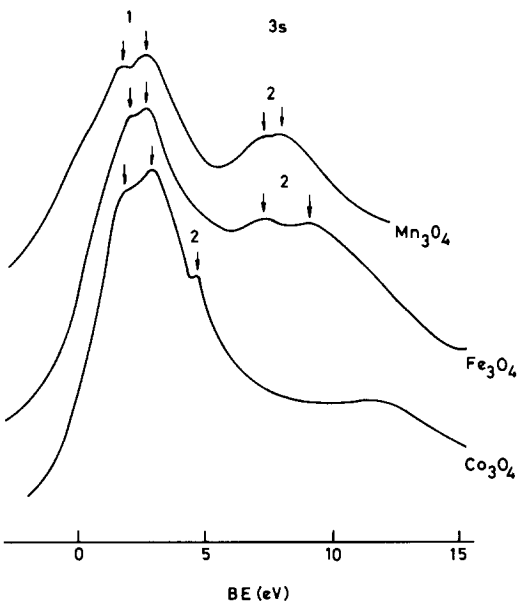

FIG. 13. X-Ray photoelectron spectra of 3*s* levels in Mn_3O_4, Fe_3O_4, and Co_3O_4 showing the coexistence of two oxidation states in these oxides. Main peaks and exchange split peaks are denoted by 1 and 2, respectively. Binding energy (BE) scale indicates only the relative energy positions of the peaks.

around 4 and 15 eV from the metal core levels, the former being shown only by the early members of the lanthanide series (*22*).

We have also found satellites appearing near the ligand core-hole spectra in the oxides of second- and third-row transition metals, as well as in the oxides of lighter first-row metals. Thus a peak around 15 eV (actual range 13.5–16.0 eV) from the main O(1*s*) peak is seen in the spectra of many of the oxides; several of these oxides also exhibit an additional peak 9 eV (actual range 8–11 eV) from the O(1*s*) peak. Intensities of satellites appearing near the O(1*s*) peak show interesting trends. In a related series of oxides of a given transition metal, the intensity increases with the decreasing number of *d* electrons for a given transition metal, having the highest value in the d^0 systems (see Fig. 14).

Satellites appearing around 4–8 eV away from the metal level peaks in compounds of Mn through Cu can be attributed to $e_g \rightarrow e_g^*$ transitions following the arguments of Kim (*28*). This essentially denotes a charge transfer from the ligand $np(e_g)$ orbital to the metal $3d(e_g^*)$ orbital due to the attractive potential at the metal site caused by the creation of a photo-hole. The contributions of the ligand and the metal orbitals to the e_g and e_g^* orbitals vary as we go across the transition metal series, and in the extreme case of Cu the $e_g \rightarrow e_g^*$ transition represents a charge transfer from the metal to the ligand (*29*).

In the case of rare earth compounds, the 4-eV satellite can be attributed to ligand *p* → metal 4*f* charge transfer excitations (*22*). The 15-eV satellite can be assigned to $O(2p)e_g \rightarrow$ metal $(5d)e_g^*$ charge transfer. We consider the 9-eV satellite in the O(1*s*) spectra to arise from the $t_{2g} \rightarrow t_{2g}^*$ transition while the 15-eV satellite is due to $e_g \rightarrow e_g^*$ excitation.

We find some systematic behavior in the intensities of the satellites described hith-

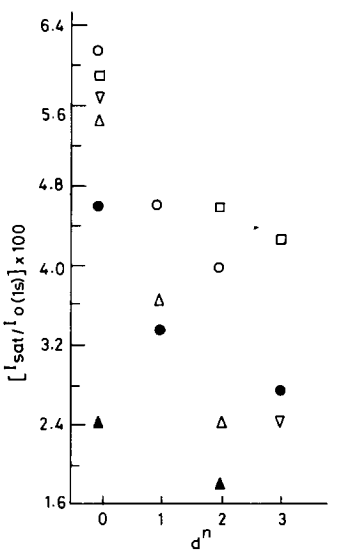

FIG. 14. Variation of the relative intensity of ligand satellite peaks (with respect to O_{1s} peak) with the number, d^n, of *d* electrons in transition metal oxides: Ti(○); V(△); Cr(□); Mn(▽); Nb(●); and Mo(▲).

erto. Thus, whenever the intensity of the metal level satellite is high (as in the compounds of Mn–Cu), the intensity of satellite next to the ligand level is generally not appreciable. Conversely, when we observe satellites in the ligand level, the intensity of the metal level is very weak. The satellites in the metal levels and the ligand levels tend to be mutually exclusive. Furthermore, we find that systems which show satellites next to the ligand levels also show interatomic Auger transitions (*30*).

The nature of the charge transfer excitation, as well as its intensity, critically depends on the metal–ligand bond covalency (or the overlap between the metal and ligand orbitals). This dependence is clearly indicated in Fig. 15, where we have plotted the intensity of the satellites of halides of Mn–Cu as a function of the ligand. From this figure we find that the satellite intensity increases with the decreasing electronegativity of the ligand in the halides of Mn, Fe, Co, and Ni; Cu halides show an opposite trend. This can be understood in terms of the assignments made earlier. In the halides of Mn–Ni, the satellite represents a charge relaxation from the ligand to the metal, and such processes are helped by less electronegative ligands. On the other hand, satellites in Cu compounds are due to charge relaxation from the metal to the ligand and consequently are helped by more electronegative ligands.

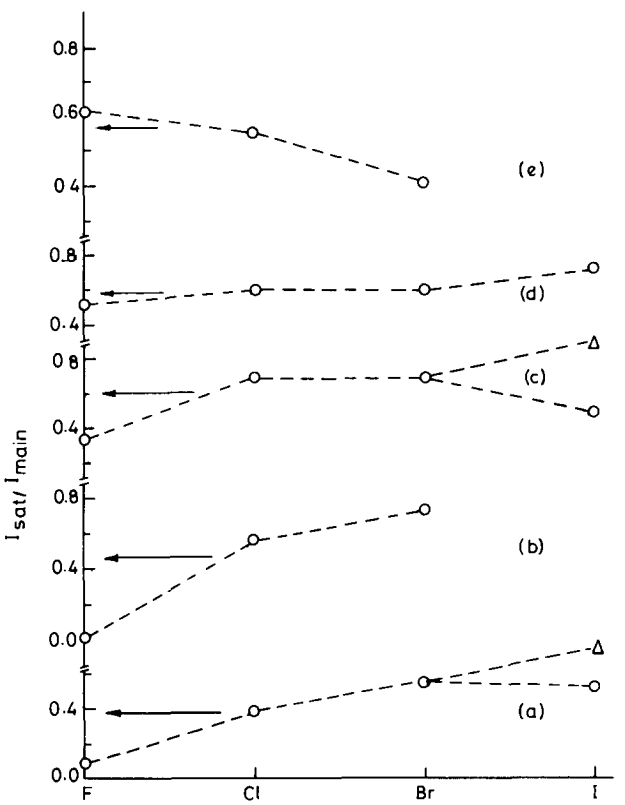

FIG. 15. Plot of relative intensity of satellites as a function of the ligand for (a) MnX_2, (b) FeX_3, (c) CoX_2, (d) NiX_2, and (e) CuX_2, where X is a halide ion. Triangles for MI_2 indicate the total intensity of satellites as obtained by adding the intensities of the two satellites that appear in these compounds only. Intensity data are taken from Ref. (*31*).

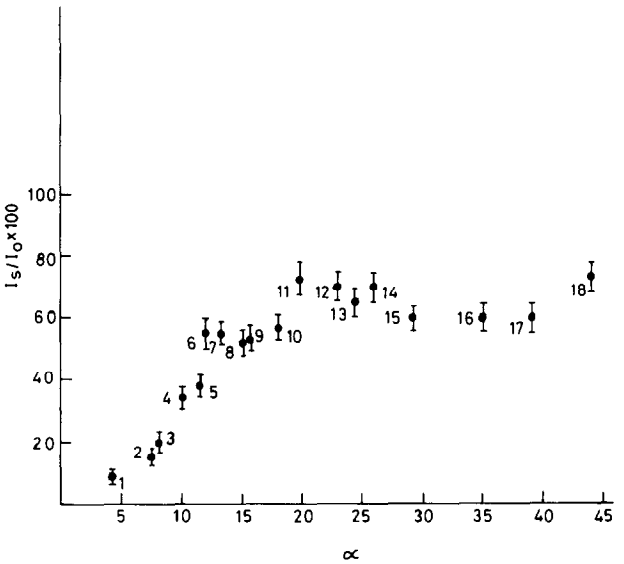

FIG. 16. Plot of the percentage relative intensity of satellites as a function of α, where α is defined as α = covalency/(10 − n), with n as the number of d electrons, for (1) MnF_2, (2) MnO, (3) FeF_3, (4) CoF_2, (5) $MnCl_2$, (6) CoO, (7) $MnBr_2$, (8) NiF_2, (9) MnI_2, (10) $FeCl_3$, (11) $FeBr_3$, (12) $CoCl_2$, (13) NiO, (14) $CoBr_2$, (15) CoI_2, (16) $NiCl_2$, (17) $NiBr_2$, and (18) NiI_2.

Although in a related series of compounds of a transition metal the satellite intensity correlates with the covalency of the bond, it has not been possible to correlate satellite intensities of various transition metal compounds with any single parameter like covalency (or orbital overlap). In our attempt to understand the parameters that govern the trends in satellite intensities in these compounds, we have plotted in Fig. 16 the satellite intensities of oxides and halides of transition metals against a parameter α defined as the ratio of covalency of the bond (calculated from Pauling electronegativities) to the number of empty d orbitals in the metal ion. It is interesting that the satellite intensity increases smoothly with α for small values of α, reaching a saturation at high values.

We have obtained rough estimates of satellite intensity in both the metal and ligand levels based on nonzero overlap of metal and ligand orbitals and sudden approximation (Fig. 17). From this figure, we see that the metal satellite intensity increases rapidly with increasing overlap for small values of the overlap, $S(<0.1)$. This explains the behavior of satellite intensity in heavier transition metal compounds (like those of Mn–Ni), as in these cases the overlap is indeed small. As overlap increases beyond S = 0.1, we find that the metal satellite intensity decreases rapidly; this explains why one finds only weak satellites in the spectra of oxides of second- and third-row transition metals, as well as of compounds of lighter first-row transition metals (like Ti), as in these cases the metal–ligand orbital overlap would be considerably larger. In the regime of very high overlap, like in the cases of sulfides and low-spin complexes of transition metals (Fe–NI), the satellite intensity becomes negligible. Figure 17 also shows the mutually exclusive nature of satellites in the ligand and the metal levels, as the ligand satellite intensity becomes considerable only when the orbital overlap between the metal and ligand becomes significantly

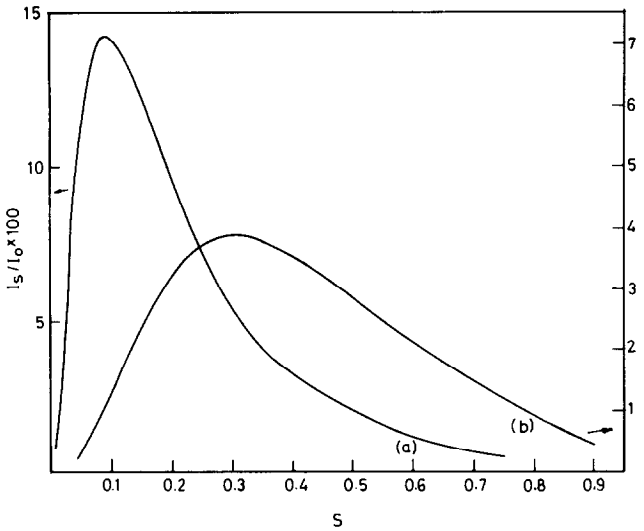

FIG. 17. Plot of calculated percentage relative intensities of the (a) metal and (b) ligand core level satellites, as a function of metal–ligand overlap.

high and consequently the metal satellite intensity gets suppressed to a considerable extent.

Valence Fluctuation in Rare Earth Systems

A host of rare earth materials exhibit valence fluctuation (or interconfigurational fluctuation) by promoting an electron to the conduction band from the $4f$ level. Typical of these are the alloys containing Ce, Sm, Eu, Tm, and Yb as a component and compounds like CeN and SmS. Systems exhibiting valence fluctuation satisfy the condition $E_{exc.} = E_n - (E_{n-1} + E_e) \sim 0$, where $(E_n - E_{n-1})$ is the energy difference between the $4f^n$ and $4f^{n-1}$ states and E_e is the energy of the promoted electron. The time scale involved in these fluctuations ($<10^{-11}$ sec) is considerably shorter than that in Mössbauer and other studies, but greater than that in XPS ($<10^{-16}$ sec). XPS is, therefore, able to show the presence of distinct valences, whereas any other study would only show the time-averaged valency of the rare earth. It has been shown that the energy separation between the different valence states in valence fluctuating systems is greater than 7 eV for $3d$ and $4d$ levels and two distinct peaks would, therefore, be expected to appear due to the two different valencies in the core level X-ray photoelectron spectra (*32*). Extensive XPS studies have been carried out on systems such as SmB_6 (*33–35*), SmS, and allied compounds (*36–38*), CeN (*39*), $CeAl_2$, and allied alloys (*40*), $CePd_3$ (*41*), $CeAl_xCo_{2-x}$ (*42*), $Eu Cu_2Si_2$ (*43*), $EuRh_{2-x}Pt_x$ (*44*), Tm chalcogenides (*45*), $YbAl_3$ (*45*), and other alloys of Yb (*46*). XPS studies of valence fluctuation systems have been briefly reviewed by Rao and Sarma (*40*).

An interesting phenomenon is found in Sm metal which is known to be in the trivalent state. Spectra of the core levels as well as of the valence band distinctly show coexistence of trivalent and divalent Sm (see Fig. 2) (*47*). Angular dependence of the intensity (*48*) and surface oxidation studies (*47*) have helped to establish that divalent Sm resides entirely on the surface, whereas the bulk metal is in the trivalent state. Such instability of the valence state on the surface is expected as the lattice relaxes near

the surface. X-Ray photoelectron spectroscopy, being highly surface sensitive, can demonstrate such phenomena which are generally inaccessible to other bulk techniques. The high surface sensitivity of electron spectroscopy can cause certain confusion as estimates of the average valency of these alloys from electron spectroscopic data are likely to be different from those obtained from other techniques. Consequently, we feel that it is important to corroborate and compliment electron spectroscopic investigations of valence fluctuation phenomena with X-ray absorption data which provide information about the bulk of the alloy and has a typical time scale similar to that of XPS. In this way, it has been possible to delineate and recognize valence instability at the surface and in the bulk in a number of Ce alloys. We show in Fig. 18 the X-ray photoelectron spectra in the $4d$ region of the $CeAl_xCo_{2-x}$ system and Fig. 19 shows the X-ray absorption spectra of the L_{III} absorption edges in the same system. Figure 18 shows that while $CeAl_2$ is entirely in the trivalent state of Ce, signals due to tetravalent species of Ce can be seen in the spectra of $CeCo_{0.4}Al_{1.6}$ and $CeCo_2$. X-Ray absorption spectra (Fig. 19) confirm the valence fluctuating nature of $CeAl_xCo_{2-x}$ for the intermediate values of x; however, $CeCo_2$ shows typical spectra due to purely tetravalent Ce. The trivalent signal seen in X-ray photoelectron spectra of $CeCo_2$ can be attributed to the existence of a surface-stabilized species or to a final state effect.

SmS is a divalent Sm alloy which undergoes a transition to the trivalent state under pressure. It is possible to induce a valence change in this compound by chemical substitution of Sm with Y, Gd, or Th (*49*). X-Ray photoelectron spectroscopic investigations show that with increasing substitution of Y or Gd in $Sm_{1-x}M_xS$ (M = Y or Gd) the lowest multiplet of divalent Sm moves toward the Fermi energy, but no trivalent Sm appears in the spectra until it reaches E_f

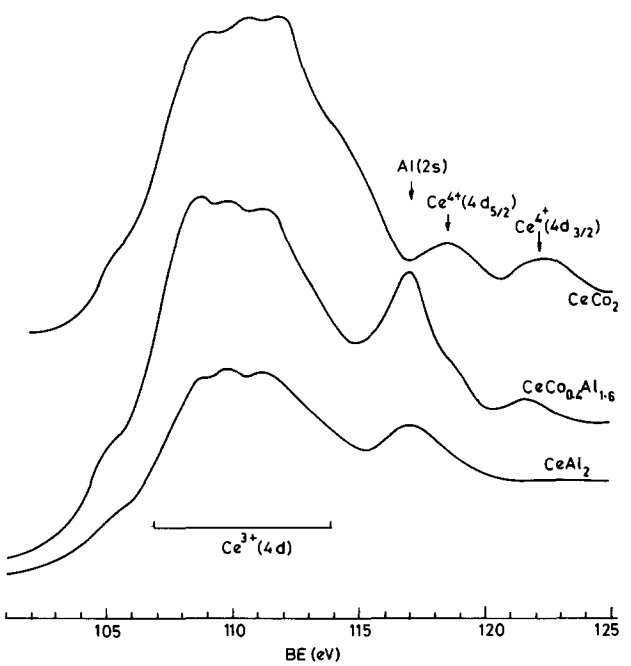

FIG. 18. X-Ray photoelectron spectra of the $4d$ region in $CeCo_xAl_{2-x}$ systems.

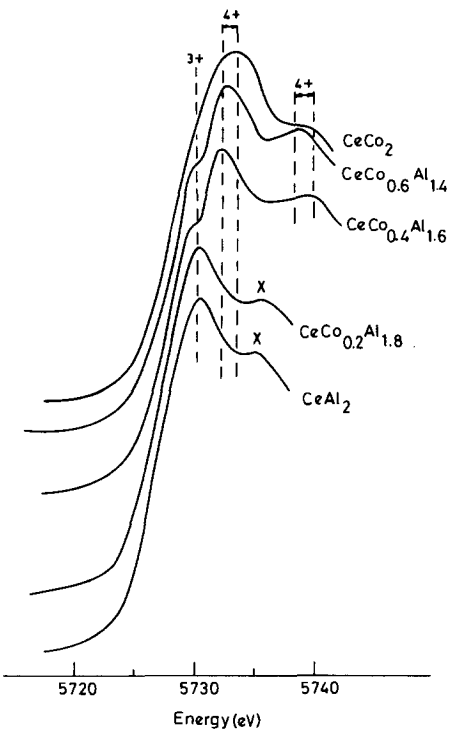

FIG. 19. L_{III} absorption edge of Ce in $CeCo_xAl_{2-x}$ system.

(*50*). Beyond this limit, further substitution of Y or Gd leads to spontaneous valence fluctuation with Sm in both divalent and trivalent states (Fig. 20). However, substitution of Ca to produce comparable changes in lattice constant does not bring about any valence transition in SmS, indicating that the valence transition in Y- or Gd-substituted SmS is of electronic origin (*49*).

Metal–Insulator Transitions

Many of the transition metal oxides exhibit thermally induced metal–insulator transitions (*51*). As such transitions are expected to be accompanied by considerable changes in the density of states in the valence band region of the oxides, they are usefully studied by photoelectron spectroscopic techniques. He I and He II, as well as X radiations, have been employed in these studies. Among the oxides of transition metals, a host of Ti and V oxides exhibit such transitions above and below the room temperature. Thus Ti_2O_3 undergoes a gradual transition in the range 300–500K from a semiconducting to a metallic phase. Accordingly, it is found (*52*) that the $3d$ band of Ti shifts gradually to lower binding energy as the temperature is raised (Fig. 21); the total shift is about 0.6 eV. VO_2 undergoes a first-order transition at 340K which manifests itself with the lowering of binding energy of V($3d$) by 0.3 eV in the metallic phase. In Ti_3O_5, the width of Ti($3d$) increases in the metallic phase. In V_2O_3, which shows two transitions at 170 and ~550K, the V($3d$) position moves to lower binding energy at room temperature compared to that at low temperature and subsequently moves to higher binding energy at higher temperature (>550K). Similar obser-

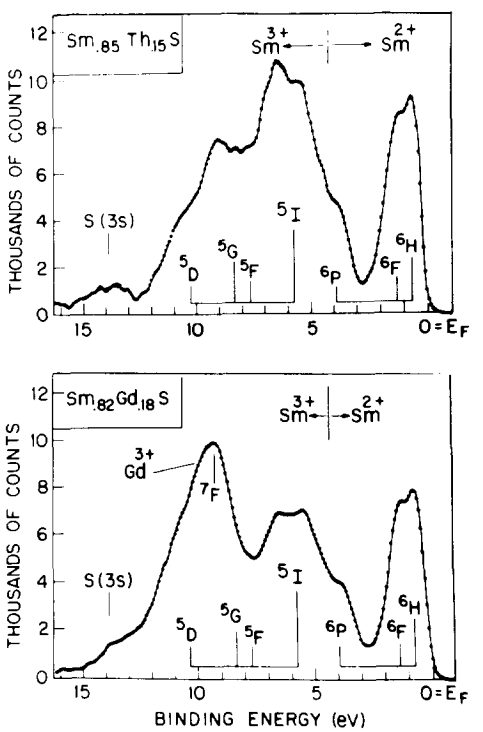

FIG. 20. X-Ray photoelectron spectra of valence band regions in $Sm_{0.85}Th_{0.15}S$ and $Sm_{0.82}Gd_{0.18}S$ [from Ref. (50)].

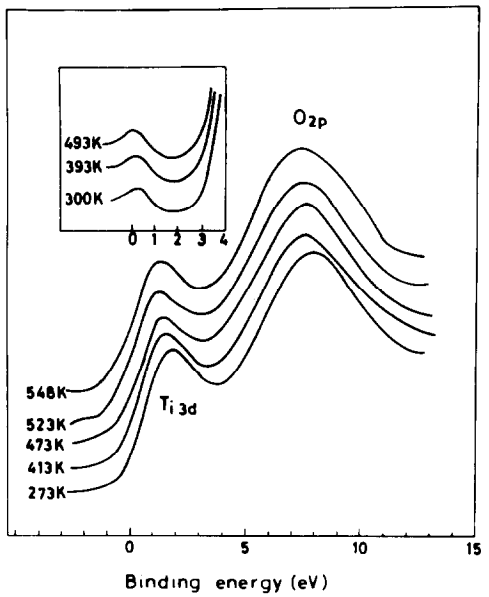

FIG. 21. X-Ray photoelectron spectra of the valence band of Ti_2O_3. Inset shows He II spectra of the Ti(3*d*) band.

vations have been made on Cr-doped V_2O_3 samples.

Photoelectron spectroscopy using He I radiation provides much higher resolution and is well suited for studying subtle changes in the valence bands of solids (*53*). He I spectra of metals, as well as metallic oxides (like TiO, VO, NbO), show a sharp cutoff in intensity at E_f as expected. This sharp cutoff is not exhibited by insulating materials. Accordingly, metallic phases of Ti_2O_3 and Ti_3O_5 show a sharp cutoff at E_f, whereas in the low-temperature semiconducting phase, the intensity rises gradually through E_f in He I photoelectron spectra (see Fig. 22). Similar observations have been made for the semiconductor–metal transitions in VO_2 and V_2O_3 (Fig. 23).

Spin-State Transitions

Transition metal ions with d^4–d^8 configuration can exist in the low- or the high-spin configurations depending on the magnitude of the crystal field splitting and the exchange energy. In particular, transitions from the low-spin to the high-spin configuration can be achieved by increasing the temperature in the case of some complexes of Fe^{2+} and Co^{3+}. Such transitions are expected to affect the valence bands as well as the core levels of the metal ions and are thus particularly suited for studying by photoelectron spectroscopic techniques. Such a study has been carried out on Fe $(phen)_2(NCS)_2$, Fe $(dipy)_2(NCS)_2$, $LaCoO_3$, and $NdCoO_3$, as well as a few model compounds where the metal ion is purely in the low-spin or in the high-spin configuration (*54*). Many differences have been observed between the spectral features of the high- and the low-spin configurations. Thus the valence band of the low-spin configuration

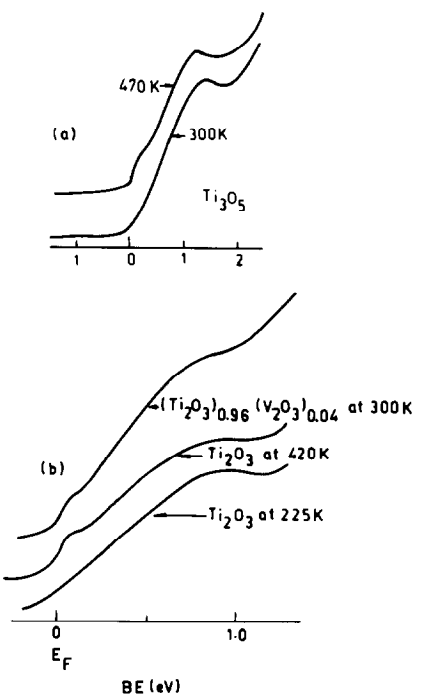

FIG. 22. (a) He I valence band of Ti_3O_5 above and below the insulator–metal transition temperature. (b) He I valence band of Ti_2O_3 above and below the insulator–metal transition temperature; the band of $(Ti_2O_3)_{0.96}(V_2O_3)_{0.04}$ which is metallic at room temperature, is shown for comparison.

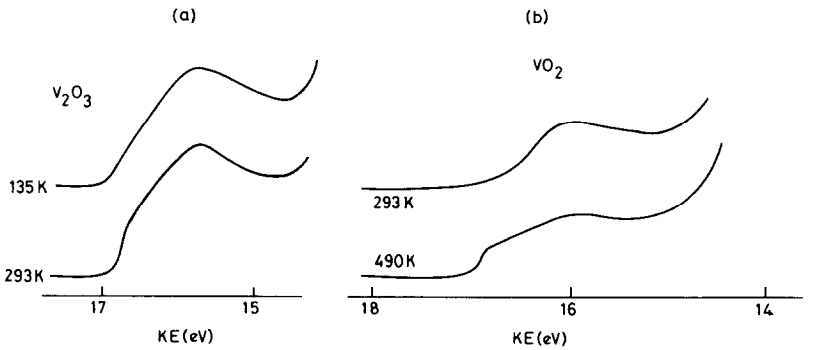

FIG. 23. He I photoelectron spectra of the V(3*d*) structure of (a) V_2O_3 and (b) VO_2 above and below the metal–insulator transition temperature showing the presence of a sharp rise in 3*d* intensity in the metallic phase [following Ref. (*53*)].

shows only one feature besides those due to O(2*p*), whereas considerable structure is seen in the high-spin case; this can be attributed to final state effects, as the low-spin configuration can achieve only one multiplet ($^2T_{2g}$) in the final state as against seven possible multiplets in the case of high-spin configuration (Table III). Moreover, low-spin configurations do not show any exchange splitting in the 3*s*-level spectra due to the absence of unpaired electrons in the valence band, whereas the high-spin configuration shows considerable exchange splitting (see Fig. 24). Similarly, satellite structures were generally seen in the core level spectra of the high-spin configurations, whereas the core levels were narrow and sharp in the low-spin cases (Fig. 24). This can be attributed to a significantly greater overlap between the ligand and metal in the case of the low-spin systems as discussed earlier.

TABLE III

FINAL STATES OF LOW-SPIN AND HIGH-SPIN d^6 IONS

Initial state	Ionized electron	Final state	Intensity
$t_{2g}^6(^1A_{1g})$	t_{2g}	$^2T_{2g}$	6
$t_{2g}^4e_g^2(^5T_{2g})$	e_g	$^4T_{1g}$	1
		$^4T_{2g}$	1
	t_{2g}	$^6A_{1g}$	6/5
		$^4A_{1g}$	2/15
		^4E	2/3
		$^4T_{1g}$	1
		$^4T_{2g}$	1

Auger Electron Spectroscopy

Auger electron spectroscopy is often used to characterize surfaces of solids. Chemical shifts of Auger signals, as well as the ratios of the intensities of the ligand (oxygen) and the metal Auger transitions, have been used for determining surface oxidation states of metals (*55*). These methods are not always useful in investigating transition metal compounds; in these systems, chemical shifts of Auger lines are generally small compared to their widths. Recently, we have shown that the ratios of the intensities of metal Auger lines can be effectively employed to study surface oxidation state of transition metal compounds (*56*). For example, we show in Fig. 25 the $L_3M_{23}M_{45}/L_3M_{23}M_{23}$ intensity ratios in the electron-beam-induced Auger spectra of titanium and vanadium oxides against the oxidation number, z, of the metal. The points corresponding to TiO_2 and V_2O_5 are not shown in the figure, since in these d^0 oxides the $L_3M_{23}M_{45}$ intensity is negligible. Although there is some scatter, the plots in Fig. 25

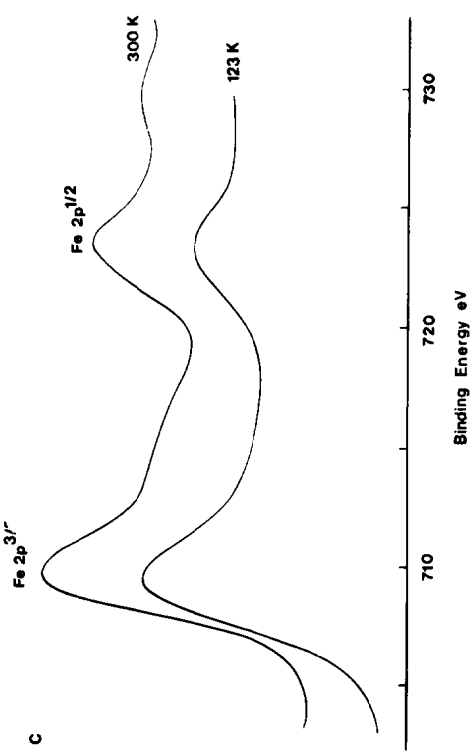

FIG. 24. (a) Fe(2*p*) bands of $K_4Fe(CN)_6$ (I) and $FeSO_4(NH_4)_2SO_4 \cdot 6H_2O$ (II). (b) Fe(3*s*) bands of I and II. (c) Fe(2*p*) bands of Fe $(phen)_2(NCS)_2$ above and below the spin-state transition temperature (174K).

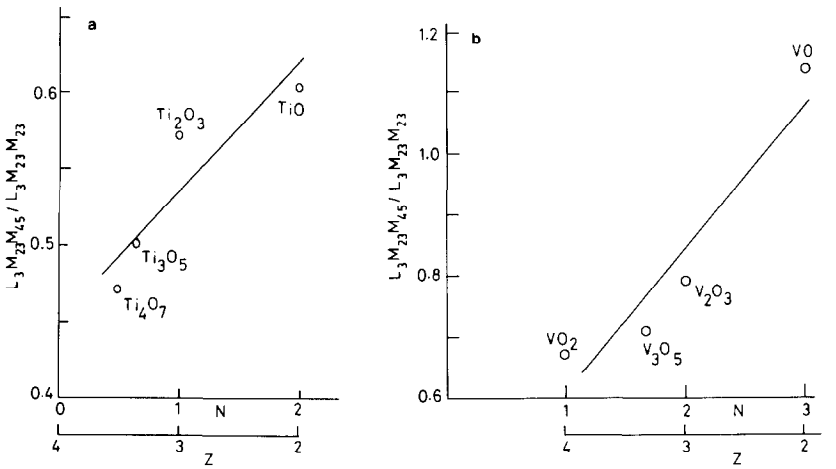

FIG. 25. Plot of $L_3M_{23}M_{45}/L_3M_{23}M_{23}$ against the number of valence electrons, N, for (a) titanium oxides and (b) vanadium oxides. The oxidation number, z, is also indicated.

indicate that this intensity ratio varies smoothly with the oxidation state of Ti and V. In Fig. 26, we show the variation of $L_3M_{45}M_{45}/L_3M_{23}M_{45}$, $L_3M_{45}M_{45}/L_3M_{23}M_{23}$, and $L_3M_{23}M_{45}/L_3M_{23}M_{23}$ intensity ratios of iron and its oxides against the oxidation number, z. The plots clearly establish that these intensity ratios vary smoothly with the oxidation number. We have further shown (*56*) that the following proportionalities hold for the transition metals and their compounds.

$$L_3M_{23}M_{45}/L_3M_{23}M_{23} \propto N,$$
$$L_3M_{45}M_{45}/L_3M_{23}M_{45} \propto (N-1),$$
$$L_3M_{45}M_{45}/L_3M_{23}M_{23} \propto N(N-1),$$

where N is the total number of valence electrons $(3d + 4s)$ in the metal. These relations are quite evident in Fig. 26, where we have indicated the values of N, $(N-1)$, and $N(N-1)$, respectively, on the ab-

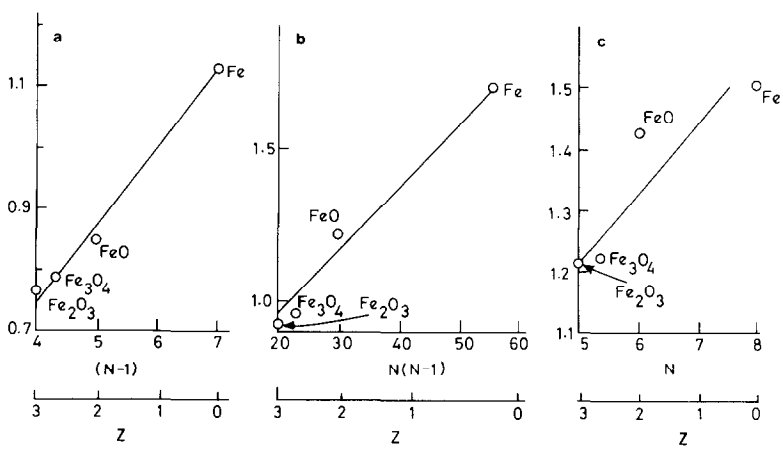

FIG. 26. Plot of (a) $L_3M_{45}M_{45}/L_3M_{23}M_{45}$ against $(N-1)$, (b) $L_3M_{45}M_{45}/L_3M_{23}M_{23}$ against $N(N-1)$, and (c) $L_3M_{23}M_{45}/L_3M_{23}M_{23}$ against N for iron and its oxides, where N is the total number of electrons at the metal site. The oxidation number, z, is also indicated.

scissa. Similar trends can be established for the oxides of Nb and Mo for the ratios $M_{45}N_{23}N_{45}/M_{45}N_{23}N_{23}$, $M_{45}N_{45}N_{45}/M_{45}N_{23}N_{45}$, and $M_{45}N_{45}N_{45}/M_{45}N_{23}N_{23}$, confirming that the above relations are generally valid. The relations indicate that metal Auger intensity ratios are indeed related to the occupancy of the valence band at the metal site and can, therefore, be used as measures of actual charge transfer from the metal to the ligand independent of the formal oxidation state of the metal. This has been confirmed by plotting the Auger intensity ratios of oxides and chalcogenides of molybdenum against the corresponding variables $(N_0 - q)$, $(N_0 - q - 1)$, and $(N_0 - q)(N_0 - q - 1)$ (Fig. 27), where N_0 is the number of valence electrons in the parent metal and q is the effective charge of the metal cation. Similar correlations have been obtained for the oxides and chalcogenides of Ni, Cu, and Zn as well.

A close examination of the Auger transitions in transition metal oxides involving the valence band has shown that oxides of the lighter transition metals show evidence of interatomic Auger transitions (*30*), contrary to the belief that interatomic Auger transitions can occur only when the intraatomic transitions are forbidden, as in highly ionic compounds like LiF and MgO (*57*). In Fig. 28, we show typical spectra of the L_3VV Auger transitions of Mn oxides and L_3M_{23}V transitions of V oxides. L_3M_{23}V transitions of titanium oxides also show evidence for interatomic Auger transitions. It can be seen from Fig. 28 that the interatomic Auger transitions become relatively more intense as the valence band of the metal gets depleted; in TiO_2 and V_2O_5, the intensity of the L_3M_{23}V transition is mostly derived from the interatomic $L_3(M)M_{23}(M)$V(O) transition as the metal (M) is in a d^0 configuration. Although the transition probability of the intraatomic mode is always greater than that of the interatomic mode, the large intensities of interatomic Auger transitions in some of the transition metal oxides indicate a large overlap between the metal and the ligand orbitals; the relative intensities of these two types of transitions are determined by the competition of the two modes of decay, the intraatomic one decreasing with increasing oxidation state of the metal. Figure 28 also indicates that the relative intensity of the

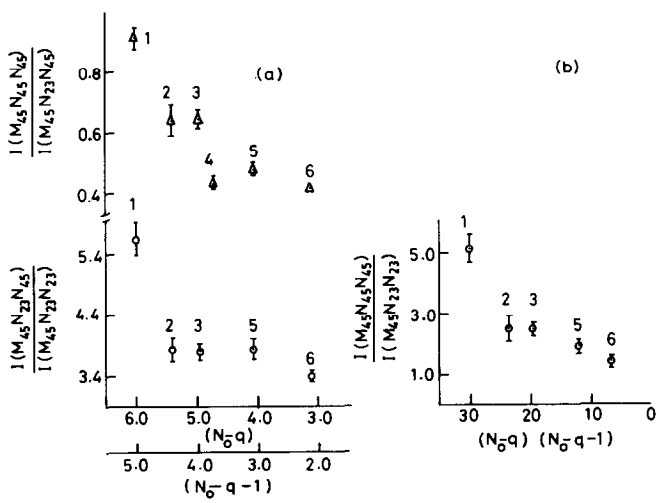

FIG. 27. Plots of (a) $M_{45}N_{23}N_{45}/M_{45}N_{23}N_{23}$ and $M_{45}N_{45}N_{45}/M_{45}N_{23}N_{45}$ and (b) $M_{45}N_{45}N_{45}/M_{45}N_{23}N_{23}$ for molybdenum chalcogenides.

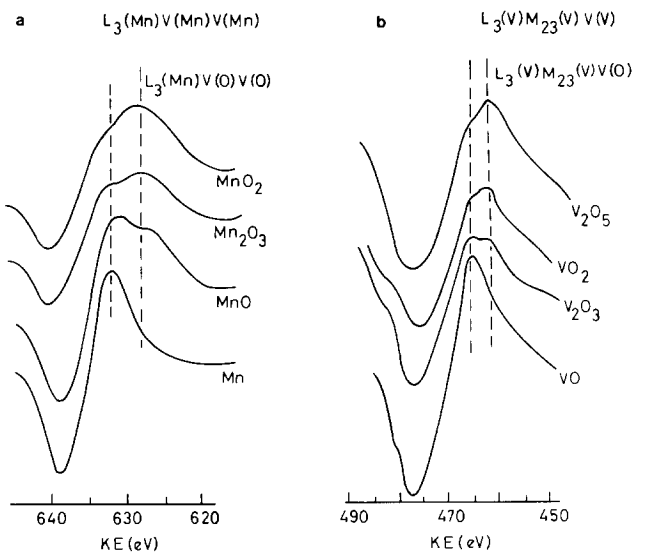

FIG. 28. (a) *LVV* intraatomic and interatomic Auger transitions in manganese oxides. (b) *LMV* intraatomic and interatomic Auger transitions in vanadium oxides.

interatomic Auger transition can be used to characterize the oxidation state of the metal.

It has been recently shown (*58–60*) that electron-, as well as photon-, stimulated desorption from metals covered with an adsorbate provides valuable information on surface layers. In this technique, O^+ ions desorb from the oxygen-covered metal surface under the impact of photons or electrons and are detected mass spectrometrically. The O^+ ion desorption involves creation of a core-hole in the metal or/and oxygen followed by Auger decay leaving holes in the valence bands. Structures observed in the O^+ ion desorption spectra provide information similar to extended X-ray absorption fine structure (EXAFS). Thus, in the case of oxygen-covered Mo, the radial distribution curves obtained from EXAFS and O^+ desorption are comparable (*58*), except for the intensity of the main peak corresponding to Mo–Mo distance. This difference in intensity is interpreted as due to the lower coordination of the metal sites on the surface compared to the bulk. Both electron- and photon-stimulated desorption studies have been employed to examine desorption of other species like OH^+ and F^+ from metal surfaces (*59*).

Electron Energy Loss Spectroscopy

In electron energy loss spectroscopy (EELS) a monochromatic beam of electrons interacts with the surface of the solid under investigation and one measures the energy of the inelastically scattered electrons. The loss in energy of the electrons contains information on the kind of excitation process undergone by the system. High-resolution EELS with low primary beam energies (~4 eV) gives valuable information on the vibrational spectra of adsorbed species, complementing the information obtained from infrared and Raman spectroscopies. Information on electronic excitations obtained from EELS using high primary beam energies (100–200 eV) is useful for understanding electron states of both the adsorbed species and the adsorbent surface.

Information on the vibrational spectra of molecules adsorbed on a surface obtained

by EELS is similar to that obtained from reflection absorption infrared spectroscopy, EELS having much greater sensitivity. Moreover, EELS provides a wider range of accessible energies compared to infrared spectroscopy, though with somewhat reduced resolution. Furthermore, there is no strict selection rule forbidding various transitions in the case of EELS. In high-resolution EELS, even a fraction of a monolayer can be detected; for example, in the case of CO adsorbed on metals, less than 0.02 monolayer has been detected.

Vibrational spectra of several molecules adsorbed on metal surfaces have been investigated by EELS and the subject has been reviewed by Rao *et al.* (*6*). Vibrational frequencies due to hydrogen adsorbed on different sites of tungsten have been analyzed in detail by Willis *et al.* (*61*). In the case of carbon monoxide adsorbed on metals, EELS gives not only the stretching frequencies due to different types of CO (linear and bridged) species, but also those due to metal carbon stretching vibrations. It is found (*62*) that a plot of ν_{C-O} of linearly adsorbed CO on metal (100) surfaces decreases as ν_{M-C} increases, implying that as the M–C bond becomes stronger, the C–O bond becomes weaker. Accordingly, ν_{C-O} decreases with increase in heat of adsorption, $\Delta H_{ads.}$. On the basis of the relation between ν_{C-O} and bond order, we find that the bond order of linearly adsorbed CO is between 2 and 3, bridged species exhibiting lower bond order.

Acetylene and ethylene adsorbed on metals have been investigated by several workers employing EELS (*6*). In both cases, a significant change in hybridization is observed, the hybridization in the adsorbed state approaching $sp^{2.5}$ or sp^3. Vibrational frequencies of molecules adsorbed on stepped sites or kinks are considerably different from those adsorbed on flat surfaces. It may be noted that identification of the adsorbed species is not altogether straightforward in some instances. Thus the nature of ethylene adsorbed on Pt(111) surface at 300K was not known for some time, but is now known to be ethylidyne (*63*).

Oxygen molecule readily dissociates on all metal surfaces except those of noble metals, Ag, Pt, and Au at low temperatures. Electron states of molecularly chemisorbed species of oxygen have been recently characterized by Rao *et al.* (*64*) on these noble metals at low temperatures by uv photoelectron and Auger electron spectroscopies. Correlating the oxygen–oxygen stretching frequencies, ν_{O-O}, of molecularly adsorbed oxygen on Ag and Pt (from EELS data) with the bond order, it is found the bond order becomes unity or less on chemisorption. This dramatic lowering of the bond order can be explained on the basis of electron donation from the metal to the π^* orbitals of the oxygen molecule, while the π orbitals may donate electrons to the metal. Such lowering of bond order is undoubtedly responsible for the dissociation of oxygen on most metals.

Electronic transitions of adsorbed molecules, as well as those pertaining to the solid surface, are readily investigated by EELS. Thus one can study interband transitions as well as transitions due to surface and bulk plasmons of metals and also examine the effect of adsorbed molecules on them. Surface plasmon loss peaks are sensitive to adsorption of molecules, particularly in the case of oxygen. A detailed review of EELS studies of electron states of adsorbed molecules may be found in the article by Rao *et al.* (*6*).

Energy loss spectra (employing high-energy electrons) of CO adsorbed on various metals show two transitions, one due to the intramolecular $1\pi + 5\sigma \rightarrow 2\pi^*$ transition and another due to the metal–ligand (π^*) charge transfer (*65, 66*). The intramolecular transition energy is essentially constant around 14 eV in all metal CO systems, while the charge transfer transition energy

varies from metal to metal. By making use of the $1\pi + 5\sigma$ binding energies on different metals from uvPS, it is possible to show that the π^* energy increases with the strength of binding (as measured by heat of adsorption). Thus both the charge transfer transition energy and the difference between the intramolecular transition energy and $1\pi + 5\sigma$ energy show similar variations with the heat of adsorption (*62*).

Since the information provided by EELS has direct bearing on the structure and stereochemistry of adsorbed species, it is useful in understanding complex phenomena like catalysis. Most studies until now have been on model systems using single crystals and the results of these studies will be of value in interpreting data on more realistic systems which may be carried out in the future. Energy loss spectra from thin crystals are being studied recently along with electron microscopy for purposes of characterization and chemical analysis. Loss spectra from surface-diffracted beams will be of value for studying surface concentration of atoms or surface states (*67*).

Concluding Remarks

The discussion hitherto shows how electron spectroscopic techniques can be fruitfully employed in the study of the electronic structures of solids and surfaces. These techniques, especially uvPS, XPS, and AES, are extremely useful for investigating densities of states, electronic transitions, and other solid state phenomena. In the case of gas–solid interactions, one can obtain information about electron states as well as vibrational states of the adsorbed species by the combined use of EELS and uvPS; at the same time, one can study the effect of the adsorbate on the adsorbent by monitoring the plasmon loss peaks and the XPS of core levels and valence bands. Studies on vibrational energy loss structure have made it possible to obtain information on the stereochemistry of surface–adsorbate systems. What is important to note is that in order to study surfaces of solids or phenomena on surfaces, it is essential to employ more than one technique. For example, in surface oxidation studies, it is desirable to employ uvPS, XPS, and AES simultaneously. Similarly, in the study of CO adsorbed on metals, uvPS and AES give information pertaining to the valence bands, and XPS provides information about the core levels; vibrational and electronic states of CO on the surface are probed by EELS. In all such studies employing single crystals, low-energy electron diffraction (LEED) provides valuable information on the surface structure.

Acknowledgment

The authors thank the Department of Science and Technology, Government of India, for support of this research.

References

1. J. M. THOMAS, *in* "Progress in Surface and Membrane Science" (J. F. Danielli and D. A. Cadenhead, Eds.), Vol. 8, p. 49, Academic Press, New York (1974).
2. C. N. R. RAO AND M. S. HEGDE, *in* "Preparation and Characterization of Materials" (J. M. Honig and C. N. R. Rao, Eds.), p. 161, Academic Press, New York (1981).
3. P. M. WILLIAMS, *in* "Handbook of X-Ray and Ultraviolet Photoelectron Spectroscopy" (D. Briggs, Ed.), p. 313, Heyden, London (1977).
4. G. K. WERTHEIM, *in* "Electron and Ion Spectroscopy of Solids" (L. Fiermans, J. Vennik, and W. Dekeyser, Eds.), p. 192, Plenum, New York (1978).
5. C. C. CHANG, *in* "Characterization of Solid Surfaces" (P. F. Kane and G. B. Larrabee, Eds.), p. 509, Plenum Press, New York (1974).
6. C. N. R. RAO, A. SRINIVASAN, AND K. JAGANNATHAN, *Int. Rev. Phys. Chem.* **1**, 45 (1981).
7. N. V. SMITH, *Phys. Rev. B* **3**, 1862 (1971).
8. J. FREEOUF, M. ERBUDAK, AND D. E. EASTMAN, *Solid State Commun.* **13**, 771 (1973).
9. S. P. KOWALCZYK, L. LEY, F. R. MCFEELY, R. A.

POLLAK, AND D. A. SHIRLEY, *Phys. Rev. B* **8**, 3583 (1973).
10. N. V. SMITH, G. K. WERTHEIM, S. HUFNER, AND M. M. TRAUM, *Phys. Rev. B* **19**, 3197 (1974).
11. N. V. SMITH, *Phys. Rev. B* **9**, 1365 (1974).
12. R. E. WATSON AND M. L. PERLMAN, *Structure Bonding* **24**, 83 (1975).
13. P. A. COX, *Structure Bonding* **24**, 59 (1975).
13a. S. F. ALVARADO, M. ERBUDAK, AND P. MUNZ, *Phys. Rev. B* **14**, 2740 (1976).
14. D. E. EASTMAN AND J. L. FREEOUF, *Phys. Rev. Lett.* **34**, 395 (1975).
15. J. GOPALAKRISHNAN, T. MURUGESAN, M. S. HEGDE, AND C. N. R. RAO, *J. Phys. C* **12**, 5255 (1979).
16. N. J. SHEVCHICK, J. TAJEDA, AND M. CARDONA, *Phys. Rev. B* **9**, 2627 (1974).
17. M. SCHLUTER AND M. L. COHEN, *Phys. Rev. B* **14**, 424 (1976).
18. F. R. SHEPHERD AND P. M. WILLIAMS, *Phys. Rev. B* **12**, 5705 (1975).
19. J. C. GREEN, *Annu. Rev. Phys. Chem.* **28**, 161 (1977).
20. P. R. SARODE, S. RAMASESHA, W. H. MADHUSUDAN, AND C. N. R. RAO, *J. Phys. C* **12**, 2439 (1979).
21. C. N. R. RAO, D. D. SARMA, S. VASUDEVAN, AND M. S. HEGDE, *Proc. Roy. Soc. London Ser. A* **367**, 239 (1979).
22. D. D. SARMA AND C. N. R. RAO, *J. Electron Spectrosc. Rel. Phenom.* **20**, 25 (1980).
23. S. VASUDEVAN, H. N. VASAN, AND C. N. R. RAO, *Chem. Phys. Lett.* **65**, 444 (1979).
24. F. R. MCFEELY, S. P. KOWALCZYK, L. LEY, AND D. A. SHIRLEY, *Phys. Lett. A* **49**, 301 (1974).
25. U. CHANDRA SINGH, D. D. SARMA, AND C. N. R. RAO, *Chem. Phys. Lett.* **85**, 278 (1982).
26. A. F. ORCHARD AND G. THORNTON, *J. Electron Spectrosc. Rel. Phenom.* **13**, 27 (1978).
27. W. C. LANG, B. D. PADALIA, L. M. WATSON, D. J. FABIAN, AND P. R. NORRIS, *Faraday Discuss. Chem. Soc.* **60**, 37 (1975).
28. K. S. KIM, *Phys. Rev. B* **11**, 2177 (1975).
29. S. LARSSON, *Chem. Phys. Lett.* **40**, 362 (1976).
30. C. N. R. RAO AND D. D. SARMA, *Phys. Rev. B* **25**, 2927 (1982).
31. G. A. VERNON, G. STUCKY, AND T. A. CARLSON, *Inorg. Chem.* **15**, 278 (1976).
32. J. F. HERBST AND J. W. WILKINS, *Phys. Rev. Lett.* **43**, 1760 (1979).
33. J. N. CHAZALVIEL, M. CAMPAGNA, G. K. WERTHEIM, AND P. H. SCHMIDT, *Phys. Rev. B* **14**, 4586 (1976).
34. J. N. CHAZALVIEL, M. CAMPAGNA, G. K. WERTHEIM, P. H. SCHMIDT, AND Y. YAFET, *Phys. Rev. Lett.* **37**, 919 (1976).
35. J. N. CHAZALVIEL, M. CAMPAGNA, G. K. WERTHEIM, AND P. H. SCHMIDT, *Solid State Commun.* **19**, 725 (1976).
36. J. L. FREEOUF, D. E. EASTMAN, W. D. GOBMAN, F. HOLTZBERG, AND J. B. TORRANCE, *Phys. Rev Lett.* **33**, 161 (1974).
37. M. CAMPAGNA, E. BUCHER, G. K. WERTHEIM, AND L. D. LONGINOTTI, *Phys. Rev. Lett.* **33**, 165 (1974).
38. R. A. POLLAK, F. HOLTZBERG, J. L. FREEOUF, AND D. E. EASTMAN, *Phys. Rev. Lett.* **33**, 820 (1974).
39. Y. BAER AND CH. ZURCHER, *Phys. Rev. Lett.* **39**, 956 (1977).
40. C. N. R. RAO AND D. D. SARMA, *in* "Science and Technology of Rare Earths" (W. E. Wallace and E. C. Subbarao, Eds.), p. 291, Academic Press, New York (1980).
41. L. C. GUPTA, E. V. SAMPATHKUMARAN, R. VIJAYARAGHAVAN, M. S. HEGDE, AND C. N. R. RAO, *J. Phys. C* **13**, L455 (1980).
42. C. N. R. RAO, D. D. SARMA, P. R. SARODE, R. VIJAYARAGHAVAN, S. K. DHAR, AND S. K. MALIK, *J. Phys. C* **14**, L 451 (1981).
43. K. H. J. BUSCHOW, M. CAMPAGNA, AND G. K. WERTHEIM, *Solid State Commun.* **24**, 253 (1977).
44. I. NOWIK, M. CAMPAGNA, AND G. K. WERTHEIM, *Phys. Rev. Lett.* **38**, 43 (1977).
45. M. CAMPAGNA, E. BUCHER, G. K. WERTHEIM, D. N. E. BUCHANAN, AND L. D. LONGINOTTI, *Phys. Rev. Lett.* **32**, 885 (1974).
46. C. N. R. RAO, D. D. SARMA, P. R. SARODE, E. V. SAMPATHKUMARAN, L. C. GUPTA, AND R. VIJAYARAGHAVAN, *Chem. Phys. Lett.* **76**, 413 (1980).
47. D. D. SARMA, M. S. HEGDE, AND C. N. R. RAO, *J. Chem. Soc. Faraday Trans. II* **77**, 1509 (1981).
48. G. K. WERTHEIM AND G. CRECELIUS, *Phys. Rev. Lett.* **40**, 813 (1978).
49. G. K. WERTHEIM, *J. Electron Spectrosc. Rel. Phenom.* **15**, 5 (1979).
50. G. K. WERTHEIM, I. NOWIK, AND M. CAMPAGNA, *Z. Phys. B* **29**, 193 (1978).
51. C. N. R. RAO AND G. V. SUBBA RAO, "Transition Metal Oxides," NSRDS Monograph No. 49, National Bureau of Standards, Washington D.C. (1974).
52. S. VASUDEVAN, M. S. HEGDE, AND C. N. R. RAO, *Solid State Commun.* **27**, 131 (1978).
53. N. BEATHAM, I. L. FRAGALA, A. F. ORCHARD, AND G. THORNTON, *J. Chem. Soc. Faraday Trans. II* **76**, 929 (1980).
54. S. VASUDEVAN, H. N. VASAN, AND C. N. R. RAO, *Chem. Phys. Lett.* **65**, 444 (1979).
55. F. J. SZALKOWSKI AND G. A. SOMORJAI, *J. Chem. Phys.* **56**, 6097 (1972).

56. C. N. R. RAO, D. D. SARMA, AND M. S. HEGDE, *Proc. Roy. Soc. London Ser. A* **370,** 269 (1980).
57. P. H. CITRIN, J. E. LOWE, AND S. B. CHRISTMAN, *Phys. Rev. B* **14,** 2642 (1976).
58. R. JAEGER, J. FELDLANS, J. HAASE, J. STOHR, Z. HUSSAIN, D. MENZEL, AND D. NORMAN, *Phys. Rev. Lett.* **45,** 1870 (1980).
59. M. L. KNOTEK AND P. J. FEIBELMAN, *Phys. Rev. Lett.* **40,** 964 (1978).
60. T. E. MADEY, *Surf. Sci.* **94,** 483 (1980).
61. R. F. WILLIS, W. HO, AND E. W. PLUMMER, *Surf. Sci.* **89,** 593 (1979).
62. C. N. R. RAO, A. SRINIVASAN, AND K. JAGANNATHAN, *Indian J. Chem. Sect. A* **20,** 72 (1981).
63. P. SKINNER, M. W. HOWARD, I. A. OXTON, S. F. A. KETTLE, D. B. POWELL, AND N. SHEPPARD, *J. Chem. Soc. Faraday Trans. II* **77,** 1203 (1981).
64. C. N. R. RAO, P. VISHNU KAMATH, AND S. YASHONATH, *Chem. Phys. Lett.* **88,** 13 (1982).
65. F. P. NETZER, R. A. WILLE, AND J. A. D. MATTHEW, *Solid State Commun.* **21,** 97 (1977).
66. G. W. RUBLOFF AND J. L. FREEOUF, *Phys. Rev. B* **17,** 4680 (1978).
67. J. M. COWLEY, *in* "Microbeam Analysis" (D. B. Wittry, Ed.), p. 33, San Francisco Press, San Francisco (1980).